

Criteria for nonlinear parameters of relativistic mean field models

A. Sulaksono^{1,4}, T. J. Bürvenich², P. -G. Reinhard³, and J. A. Maruhn⁴

¹*Departemen Fisika, FMIPA, Universitas Indonesia, Depok, 16424, Indonesia*

²*Frankfurt Institute for Advanced Studies,*

Universität Frankfurt, 60438 Frankfurt am Main, Germany

³*Institut für Theoretische Physik II,*

Universität Erlangen-Nürnberg, D-91058 Erlangen, Germany

⁴*Institut für Theoretische Physik, Universität Frankfurt,*

60438 Frankfurt am Main, Germany

Abstract

Based on the properties of the critical and the actual effective masses of sigma and omega mesons, criteria to estimate the values of the isoscalar nonlinear terms of the standard relativistic mean field model that reproduce stable equations of state in respect to particle hole excitation at high densities are derived. The relation between nuclear matter stability and the symmetric nuclear matter properties are shown. The criteria are used to analyze in a more systematic way the high-density longitudinal and transverse instabilities of some parameter sets of relativistic mean field models. The critical role of the vector and vector-scalar nonlinear terms is also discussed quantitatively.

PACS numbers: 21.30.Fe, 21.65.+f, 21.60.-n

I. INTRODUCTION

Relativistic mean field (RMF) models have been quite successful in providing a microscopic description of many ground-state properties from medium to heavy nuclei. The parameters of each model are obtained by adjusting its parameters to a few ground-state properties of a set of magic and semi-magic nuclei. The differences between one parameter set and the others are not only due to differences in choosing observables, strategies, and constraints for the parametrization, but also to the difference in the nonlinear ansatz used. Even in recent years, there have still been some efforts to generate new RMF parameter sets [1, 2, 3, 4]. The aim is to improve and to extend the applicability of the model for the description not only of ground states but also of excited states of finite nuclei and nuclear matter. Indeed, even the boundaries are not too clear, the range of applicability of RMF models is limited. Therefore, applying the models in regions which are outside their fitting window by extrapolation needs special care.

Recently, considerable attention has been paid in constraining the equation of state (EOS) of matter beyond the nuclear matter saturation density (ρ_0) using flow data from heavy-ion collision experiments and astrophysical observatories [5, 6, 7]. In order to be consistent with data, the EOS should be relatively soft at moderate densities ($\leq 5\rho_0$) and stiff at high densities ($> 5\rho_0$). Many models, including some parameter sets of RMF models have been checked. The author of Ref. [7], also used some model independent calculations of pure neutron matter as an additional theoretical constraint to test the validity of two parameter sets of RMF models (NL3 and FSUGold) at high densities. It is found that FSUGold is consistent with all constraints except for a high density EOS that appears mildly softer than required by astronomical observations [7]. It seems that some parameter sets of RMF models are unable to fulfil the above requirements [5, 6, 7]. At this point, we have sufficient reason to re-investigate the parameterizations of RMF models with high density applications in mind.

We studied the high density instabilities of some representative parameter sets of RMF models with respect to density fluctuation by observing their longitudinal and transverse particle-hole excitation modes [8]. We have found that certain parameter sets are unstable at high densities but for some parameter sets with additional vector and vector-scalar nonlinear terms, the onset of instabilities can be pushed into a region with quite large matter density

(ρ_B) and perturbed momenta (q). It means that the longitudinal and transverse parts of the particle-hole excitation modes of relativistic mean field models depend sensitively on the isoscalar nonlinear terms used. Therefore by adjusting these nonlinear terms, the instabilities at high densities of RMF models can be avoided.

In this work, we extend the results of our previous letter [8] by deriving criteria to estimate the values of isoscalar nonlinear terms of the standard RMF model (RMF model with minimal nonlinear terms) that produce a stable EOS at high densities. We then employ these criteria to systematically study the high density longitudinal and transverse instabilities of some representative RMF models. In this way, the actual role of vector and scalar-vector nonlinear terms can be revealed in a more quantitative manner. These analyses can provide a practical hint that should be useful for RMF parameterization. The extension to the isovector sector is also important. The question whether the parameter set of the standard RMF model with stable nuclear matter EOS at high densities is consistent with the above constraints and simultaneously has acceptable predictions for finite nuclei, would also be very interesting to investigate, but these points need additional considerations that are beyond the scope of this work and will left to a future paper.

This paper is organized as follow: in Sec. II it is discussed how to estimate the isoscalar nonlinear parameter sets of the standard RMF model; in Sec. III we discuss the stability of some RMF models; and finally in Sec. IV the conclusions are drawn.

II. CONSTRAINING NONLINEAR PARAMETERS OF STANDARD RELATIVISTIC MEAN FIELD MODELS

The instability of nuclear matter at high density is generated by particle-hole excitation modes. These modes are indicated by the existence of poles of the meson propagators at zero energy transfer. [9, 10, 11]. In this section, the criteria for the isoscalar nonlinear parameter values of the relativistic mean field model that cause instabilities at relatively high densities are investigated.

We start from the energy density ε of standard RMF models in symmetric nuclear matter (SNM) as,

$$\varepsilon = \varepsilon_{\text{linear}} + \frac{1}{3}b_2\sigma^3 + \frac{1}{4}b_3\sigma^4 - \frac{1}{4}c_3V_0^4, \quad (1)$$

where $\varepsilon_{\text{linear}}$ is the energy density of the linear Walecka model. Note that from now on, we denote parameter sets with nonlinear vector parameter $c_3=0$ as S-RMF, and those with this parameter not equal to zero as V-RMF. The transverse (ϵ_T) and longitudinal (ϵ_L) dielectric functions at $q_0 = 0$ for SNM are [8]

$$\begin{aligned}\epsilon_T &= 1 + 2d_V^T \Pi_T, \\ \epsilon_L &= 1 + 2d_S \Pi_S - 2d_V^L \Pi_V,\end{aligned}\tag{2}$$

with the effective vector polarization defined as

$$\Pi_V \equiv \Pi_{00} - 2d_S \Pi_M^2 + 2d_S \Pi_S \Pi_{00}.\tag{3}$$

The explicit forms of the polarizations are

$$\begin{aligned}\Pi_T(q, 0) &= \frac{1}{\pi^2} \left\{ \frac{1}{6} k_F E_F - \frac{q^2}{6} \ln \frac{k_F + E_F}{M^*} \right. \\ &\quad \left. - \frac{E_F}{6q} (2M^{*2} - k_F^2 - \frac{3}{4} q^2) \ln \left| \frac{2k_F - q}{2k_F + q} \right| - \frac{E}{3q} (M^{*2} - \frac{1}{2} q^2) \ln \left| \frac{qE_F - 2k_F E}{qE_F + 2k_F E} \right| \right\},\end{aligned}\tag{4}$$

for the transverse polarization,

$$\begin{aligned}\Pi_S(q, 0) &= \frac{1}{2\pi^2} \left\{ k_F E_F - (3M^{*2} + \frac{q^2}{2}) \ln \frac{k_F + E_F}{M^*} \right. \\ &\quad \left. + \frac{2E_F E^2}{q} \ln \left| \frac{2k_F - q}{2k_F + q} \right| - \frac{2E^3}{q} \ln \left| \frac{qE_F - 2k_F E}{qE_F + 2k_F E} \right| \right\},\end{aligned}\tag{5}$$

for the scalar polarization,

$$\Pi_M(q, 0) = \frac{M^*}{2\pi^2} \left\{ k_F - \left(\frac{k_F^2}{q} - \frac{q}{4} \right) \ln \left| \frac{2k_F - q}{2k_F + q} \right| \right\},\tag{6}$$

for the mixed scalar-vector polarization, and

$$\begin{aligned}\Pi_{00}(q, 0) &= -\frac{1}{\pi^2} \left\{ \frac{2}{3} k_F E_F - \frac{q^2}{6} \ln \frac{k_F + E_F}{M^*} - \frac{E_F}{3q} (M^{*2} + k_F^2 - \frac{3q^2}{4}) \ln \left| \frac{2k_F - q}{2k_F + q} \right| \right. \\ &\quad \left. + \frac{E}{3q} (M^{*2} - \frac{q^2}{2}) \ln \left| \frac{qE_F - 2k_F E}{qE_F + 2k_F E} \right| \right\},\end{aligned}\tag{7}$$

for the longitudinal polarization, with Fermi momentum k_F , nucleon effective mass $M^* = M - g_\sigma \sigma$, Fermi energy $E_F = (k_F^2 + M^{*2})^{1/2}$, and $E = (q^2/4 + M^{*2})^{1/2}$.

The longitudinal scalar meson propagator is given by

$$d_S = \frac{g_\sigma^2}{q^2 + m_\sigma^{*2}}, \quad (8)$$

while the vector meson longitudinal and transverse propagators are

$$d_V^L = d_V^T = \frac{g_\omega^2}{q^2 + m_\omega^{*2}}, \quad (9)$$

where the σ and ω mesons effective masses are given by

$$\begin{aligned} m_\sigma^{*2} &= \frac{\partial^2 \epsilon}{\partial^2 \sigma} = m_\sigma^2 + 2b_2 \sigma + 3b_3 \sigma^2, \\ m_\omega^{*2} &= -\frac{\partial^2 \epsilon}{\partial^2 V_0} = m_\omega^2 + 3c_3 V_0^2. \end{aligned} \quad (10)$$

If we define m_σ^{*2c} and m_ω^{*2c} as m_σ^{*2} and m_ω^{*2} at $\epsilon_T=0$ and $\epsilon_L=0$ simultaneously, then from Eqs. (2, 8 and 9) we have

$$\begin{aligned} m_\omega^{*2c} &= -[2g_\omega^2 \Pi_T + q^2], \\ m_\sigma^{*2c} &= -\left[\frac{2g_\sigma^2 (\Pi_S \Pi_T - \Pi_M^2 + \Pi_S \Pi_{00})}{(\Pi_T + \Pi_{00})} + q^2 \right]. \end{aligned} \quad (11)$$

Because the presence of poles in the meson propagators is equivalent with $\epsilon_T=0$ and $\epsilon_L=0$, it implies that at any nuclear matter density and momentum q , the stable regions are determined from the following criteria

$$\begin{aligned} \frac{m_\sigma^{*2c}}{m_\sigma^{*2}} &< 1, \\ \frac{m_\omega^{*2c}}{m_\omega^{*2}} &< 1. \end{aligned} \quad (12)$$

We observe that the m_σ^{*2c} and m_ω^{*2c} of every RMF parameter set strongly depend on the values of g_σ and g_ω but are insensitive to the values of the parameters b_2 , b_3 , and c_3 . In the contrary, m_σ^{*2} and m_ω^{*2} do not depend explicitly on g_σ and g_ω values but they are very sensitive to the values of b_2 , b_3 , and c_3 . Fortunately, we also observe that most of the standard RMF parameter sets in the literature's with acceptable predictions for nuclear matter and finite nuclei have similar g_σ and g_ω values. Let us take the average values of both coupling constants as the “standard” values of both parameters. We found that, for any parameter set, if the values of these g_σ and g_ω parameters are larger than the standard

TABLE I: Isoscalar parameters for some test parameter sets.

| Parameter | test1 | test2 | test3 | test4 | test5 |
|------------|--------|-------|-------|-------|--------|
| g_σ | 10.08 | 10.18 | 10.02 | 10.02 | 10.03 |
| g_ω | 12.62 | 12.64 | 12.62 | 12.63 | 12.62 |
| b_2 | -10.53 | -7.10 | -7.00 | -6.80 | -6.83 |
| b_3 | -28.00 | -3.80 | 0.00 | 3.80 | 20.00 |
| c_3 | 0.29 | 56.77 | 70.77 | 84.71 | 159.70 |

ones, its $m_\sigma^{*2/c}$ and $m_\omega^{*2/c}$ are higher and on the other hand, if these coupling constants are smaller, its $m_\sigma^{*2/c}$ and $m_\omega^{*2/c}$ are lower.

Based on the fact that almost all of the standard RMF parameter sets in the literature have similar values of g_σ and g_ω , we will use Eq. (12) to determine a lower limit for the b_2 , b_3 , and c_3 parameters of standard RMF models that are stable with respect to the particle-hole excitation modes at high densities. For the transverse mode, it is relatively straightforward to extract one parameter c_3 from a critical effective omega meson mass, but for the longitudinal one, to pick up two parameters b_2 and b_3 from a critical effective sigma meson mass can generate many combinations because the correlation between b_2 and b_3 for each parameter set is different. It depends on many factors, like the values of other parameters, fitting procedure and strategy including the choice of observables for parameterization etc. To avoid this problem, we generate some test parameter sets with almost the same value of g_σ and g_ω with variation of b_3 (the b_3 term dominates over the b_2 term at high densities) while the b_2 and c_3 parameters are adjusted such that the standard SNM properties at saturation are fulfilled. The parameters of some exemplary test parameter sets can be seen in Table I. The SNM binding energy and pressure predicted by each test parameter in this table are displayed in Fig. 1, while their ratios of effective mass to nucleon mass and the compressibilities are shown in Fig. 2. It is clear from both pictures that they have similar nuclear matter properties at saturation (insets) but are different at high densities. The EOS of parameter sets with $b_3 \geq 0$ tends to be closer to the one of the experimental data from Ref. [12] and the microscopic calculation of Ref. [13].

In Fig. 3, the ratio of the critical effective meson masses to the effective meson masses is shown. The connection of the b_3 parameter set with the appearance of instabilities is clearly

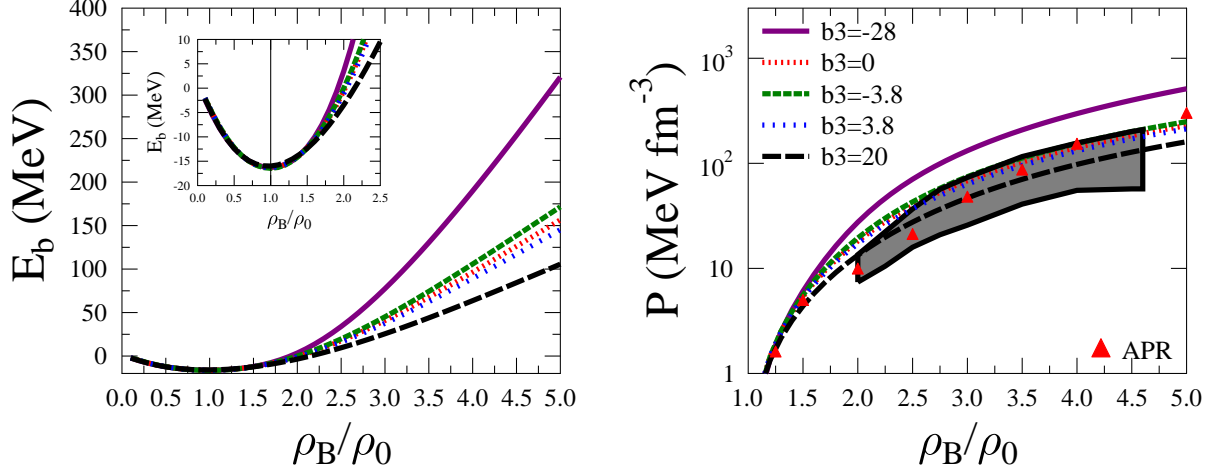


FIG. 1: The SNM binding energy (left panel) and pressure (right panel) calculated using test parameter sets in Table I. The Shaded region in the right panel corresponds to experimental data of Ref. [12], and the triangles to data calculated from the microscopic model of Ref. [13]. The inset figure shows the low-density region at better resolution.

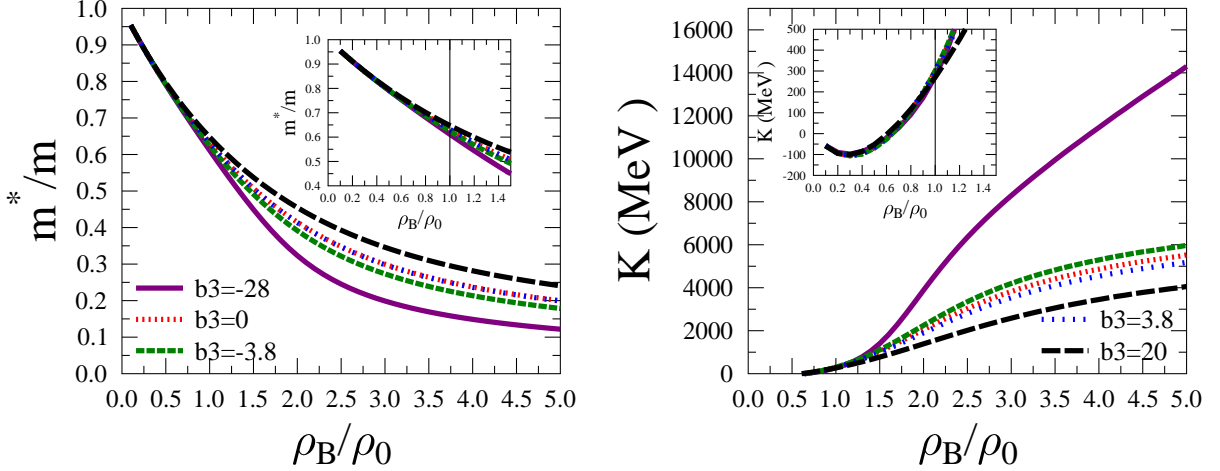


FIG. 2: The SNM nucleon effective mass (left panel) and compressibility (right panel) calculated using the test parameter sets of Table I. The inset figure shows the low-density region at better resolution.

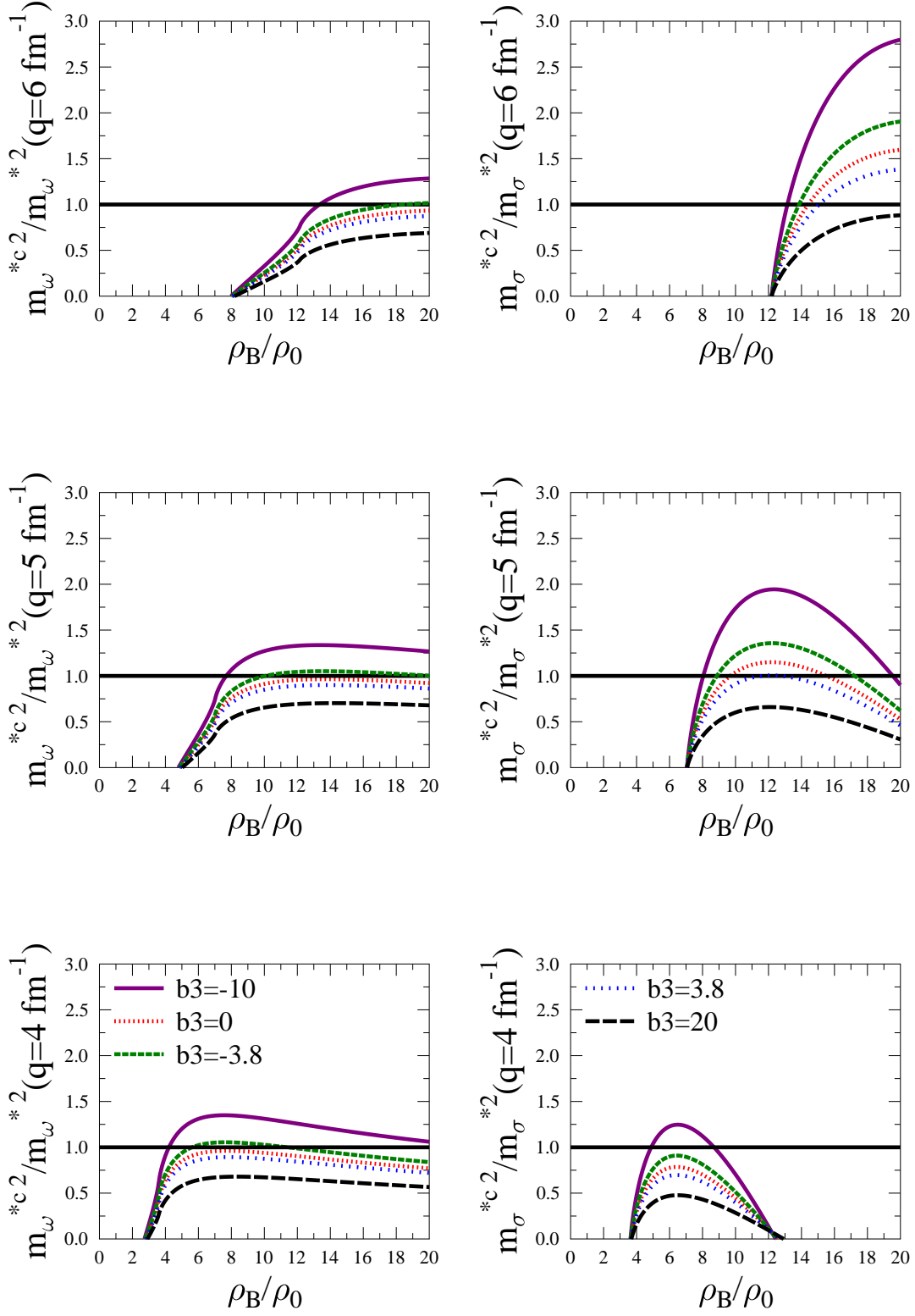


FIG. 3: $m_{\sigma}^{*2c}/m_{\sigma}^{*2}$ and $m_{\omega}^{*2c}/m_{\omega}^{*2}$ as functions of ρ_B/ρ_0 for various values of q and b_3 as indicated.

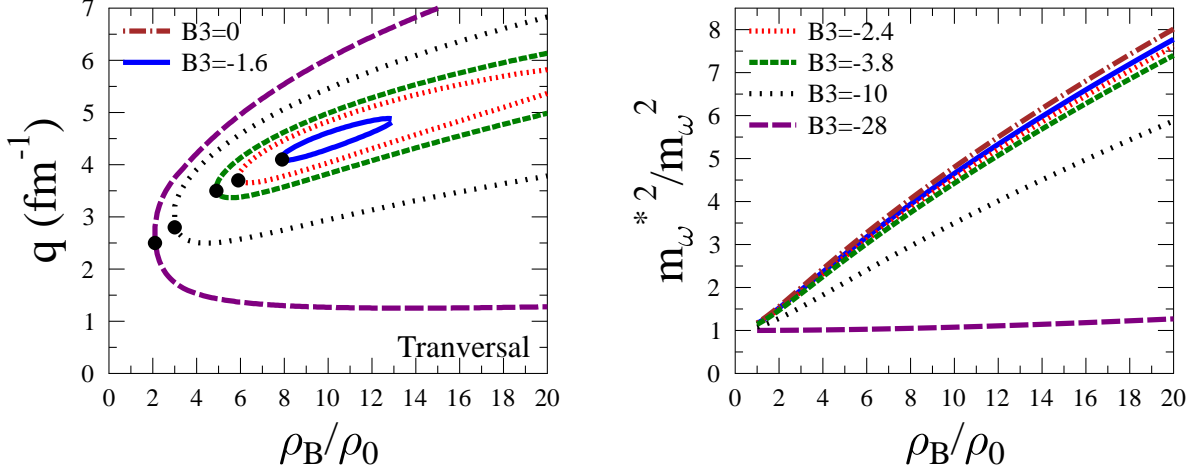


FIG. 4: The onset of transverse instability (in the left panel) and effective omega meson mass (in the right panel) for some test parameter sets. The dot markers show their critical densities.

captured. The explicit relation of the onset of transverse instability with effective omega meson mass can also be seen in Fig. 4 and the one of the longitudinal mode is shown in Fig. 5. Fig. 4 shows the correlation between transverse instability and the effective mass of the omega meson which depends strongly on the vector nonlinear term. By comparing Fig. 6 with the values of c_3 and b_3 in Table I, it is clear that every parameter set with $c_3 > 71$ does not show a transverse instability region at high density. To attain this value for c_3 , it seems that we need b_3 close to or larger than zero.

On the other hand, we can see from Fig. 5 that the longitudinal instability can be related to the effective sigma meson mass which strongly depends on scalar nonlinear terms. The longitudinal instability cannot fully disappear, but can be pushed to unphysical densities by taking b_3 relatively large and positive, for example, $b_3 \geq 20$, which it corresponds to the value of $c_3 \geq 160$. In this case, the onset of instability can be pushed to $\rho_c \geq 23\rho_0$. For high-density applications (neutron stars, supernova matter, etc.) the maximum density is $10\rho_0$, with ρ_0 the SNM saturation density. This shows that for the purpose of these applications the parameter set with $b_3 > 0$ may be sufficient. For negative but relatively large absolute values of b_3 , an additional onset of longitudinal instability is generated. This appears due to the effective sigma meson mass becoming imaginary after reaching a certain

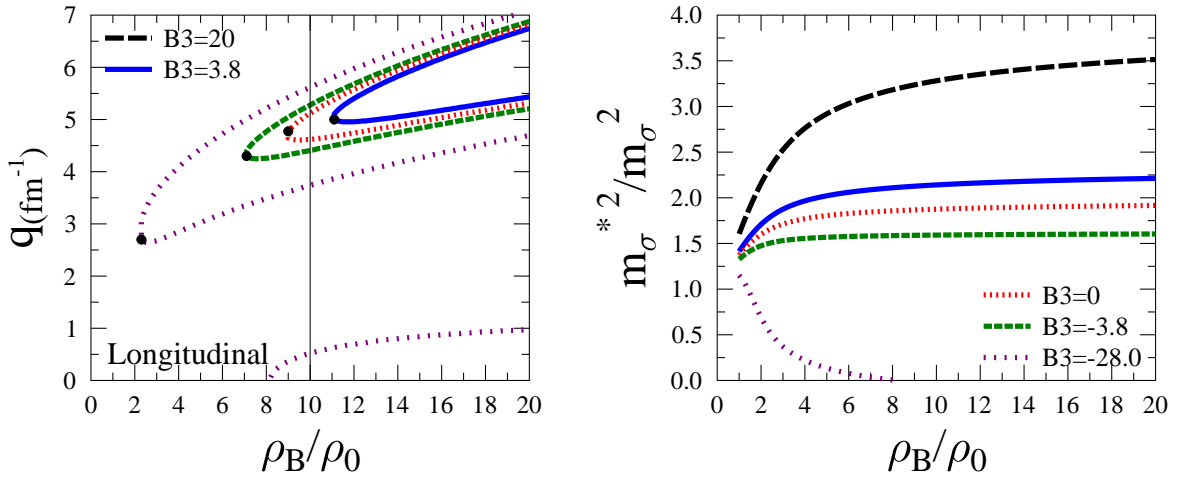


FIG. 5: The onset of longitudinal instability (in the left panel) and effective sigma meson mass (in the right panel) for some test parameter sets. The dot markers show their critical densities.

critical density. This instability appears if $b_3 \leq -28$. These results can be also directly seen from Fig. 3. Of course for arbitrary standard RMF parameter sets, its value can be relatively lower or higher, depending on how large the value of b_2 is. Once again, we need to emphasize that the critical nonlinear parameters are obtained using “standard” g_ω and g_σ . Therefore for parameter sets with g_ω and g_σ deviating appreciably from these, their critical nonlinear parameters can be smaller or larger.

The last finding here is that the parameter sets which are stable at high densities are consistent with the experimental data of Ref. [12] and the microscopic calculation of Ref. [13] with respect to their SNM EOS.

III. ANALYZING THE STABILITY OF SOME RELATIVISTIC MEAN FIELD MODELS

Here we will use the criteria defined in the previous section to analyze more systematically the high density longitudinal and transverse instabilities of some RMF models. The onset of instabilities of some parameter sets have been reported in Ref. [8], but the discussion there was not quite robust. Therefore, in this work, we need to elucidate one point that was not

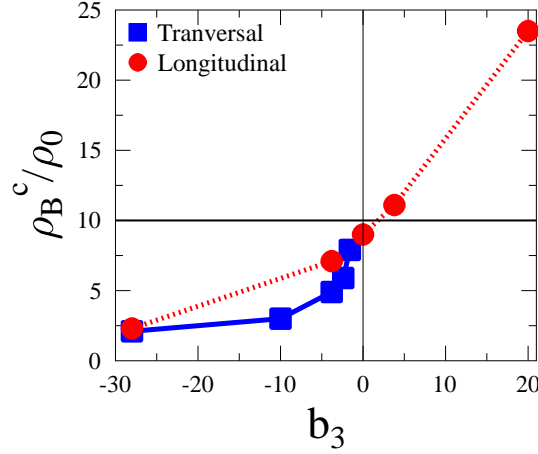


FIG. 6: The ratio between critical and saturation densities as a function of the b_3 parameter for both modes.

treated properly in Ref. [8], namely that both instabilities are determined by the interplay between critical and actual effective meson masses (Eq. (12)). To comprehend our previous results [8], now we also enlarge the number of parameter sets used.

A. Standard relativistic mean field models

First, we start with S-RMF. We select four parameter sets of this model as representative, i.e., NLZ [14], NL3 [15], NLSH [16] and NL2 [17]. The isoscalar parameters of these parameter sets can be seen in Table II. It can be seen that g_σ and g_ω are of similar magnitude for NLZ, NL3, and NLSH, but the ones of NL2 are significantly smaller. Therefore, the parameter sets NLZ, NL3, and NLSH have similar σ and ω critical effective masses while those of NL2 are smaller. Because NL2 has σ and ω critical effective masses which are smaller than for the others and a positive value of the b_3 parameter, the longitudinal instability of this parameter set disappears in the range of densities and q values used. On the other hand NLSH, having a quite large b_2 parameter and a moderate b_3 parameter, its sigma meson effective mass is larger compared to the ones of NLZ and NL3. Therefore, its instability regions are narrower and have no fluctuations. All parameter sets of S-RMF have a transverse instability. At relatively small q ($\leq 4 \text{ fm}^{-1}$), they start to appear in quite low

TABLE II: Isoscalar parts of some S-RMF model parameter sets.

| Parameter | NLZ | NL3 | NLSH | NL2 |
|------------|--------|--------|--------|-------|
| g_σ | 10.05 | 10.22 | 10.44 | 9.11 |
| g_ω | 12.91 | 12.86 | 12.95 | 11.49 |
| b_2 | -13.51 | -36.12 | -6.91 | -2.30 |
| b_3 | -40.22 | -10.43 | -15.83 | 13.78 |
| c_3 | 0 | 0 | 0 | 0 |

TABLE III: Isoscalar parts of some V-RMF model parameter sets.

| Parameter | NLSV1 | PK1 | TM1 | NLSV2 | Z271 | FSUGold |
|------------|--------|--------|-------|-------|-------|---------|
| g_σ | 10.12 | 10.32 | 10.03 | 10.32 | 7.03 | 10.59 |
| g_ω | 12.73 | 13.01 | 12.61 | 12.88 | 8.41 | 14.30 |
| b_2 | -9.24 | -8.17 | -7.23 | -6.86 | -5.43 | -4.28 |
| b_3 | -15.39 | -10.00 | 0.62 | 0.37 | 63.69 | 49.93 |
| c_3 | 41.01 | 55.65 | 71.33 | 72.39 | 49.94 | 418.39 |

densities. These facts are clearly depicted in Fig. 7.

Next, we will discuss the V-RMF model. Here, we investigate the parameter sets NLSV1 and NLSV2 of Ref. [18], TM1 [19], PK1 [20], Z271 [21], and FSUGold [4]. The isoscalar parameters of these parameter sets can be seen in Table III. Due to the small values of the g_σ and g_ω coupling constants for the Z271 parameter set, it has relatively small σ and ω critical effective masses, so that even though its $c_3 < 71$, the parameter set Z271 does not have a transverse instability region. On the other hand, for the TM1, NLSV2, and FSUGold parameter sets, their transversal instabilities disappear due to the fact that these parameter sets have $c_3 > 71$. In the V-RMF model, it is very clear reflected that, if b_3 becomes smaller then its longitudinal instability region becomes larger. This fact can be understood by comparing Fig. 8 with the b_3 values in Table III.

In general, the problem of the transverse part of S-RMF maybe can remedied by using very large bare omega meson masses but this still leaves the problem in the longitudinal part that should be fixed. Many parameter sets of the S-RMF model have negative but relatively large absolute value of b_3 . This fact leads to the situation that after reaching a certain

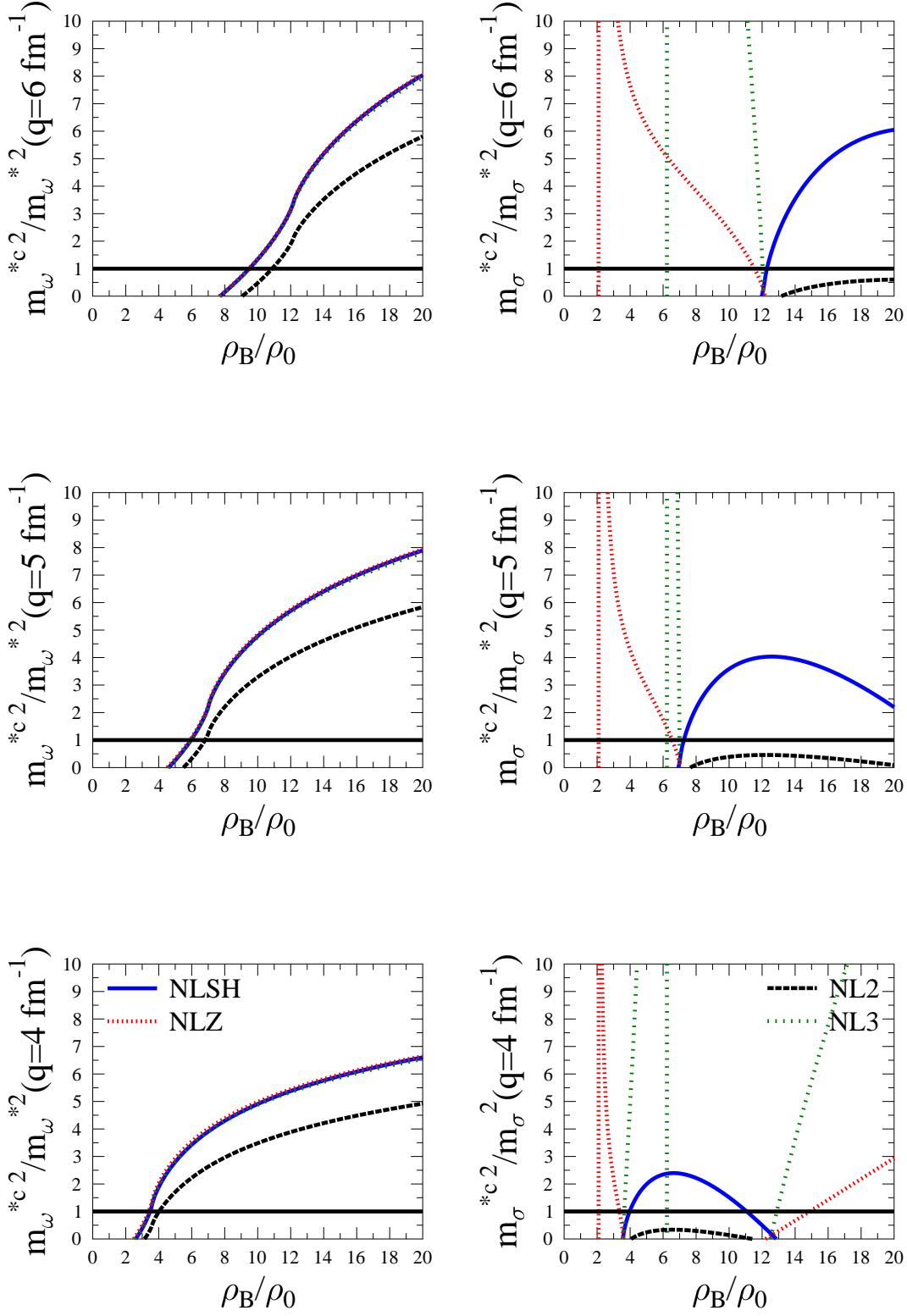


FIG. 7: $m_\sigma^{*2} c / m_\sigma^{*2}$ and $m_\omega^{*2} c / m_\omega^{*2}$ for some S-RMF parametrizations in Table II as functions of ρ_B / ρ_0 , with q varying as indicated.

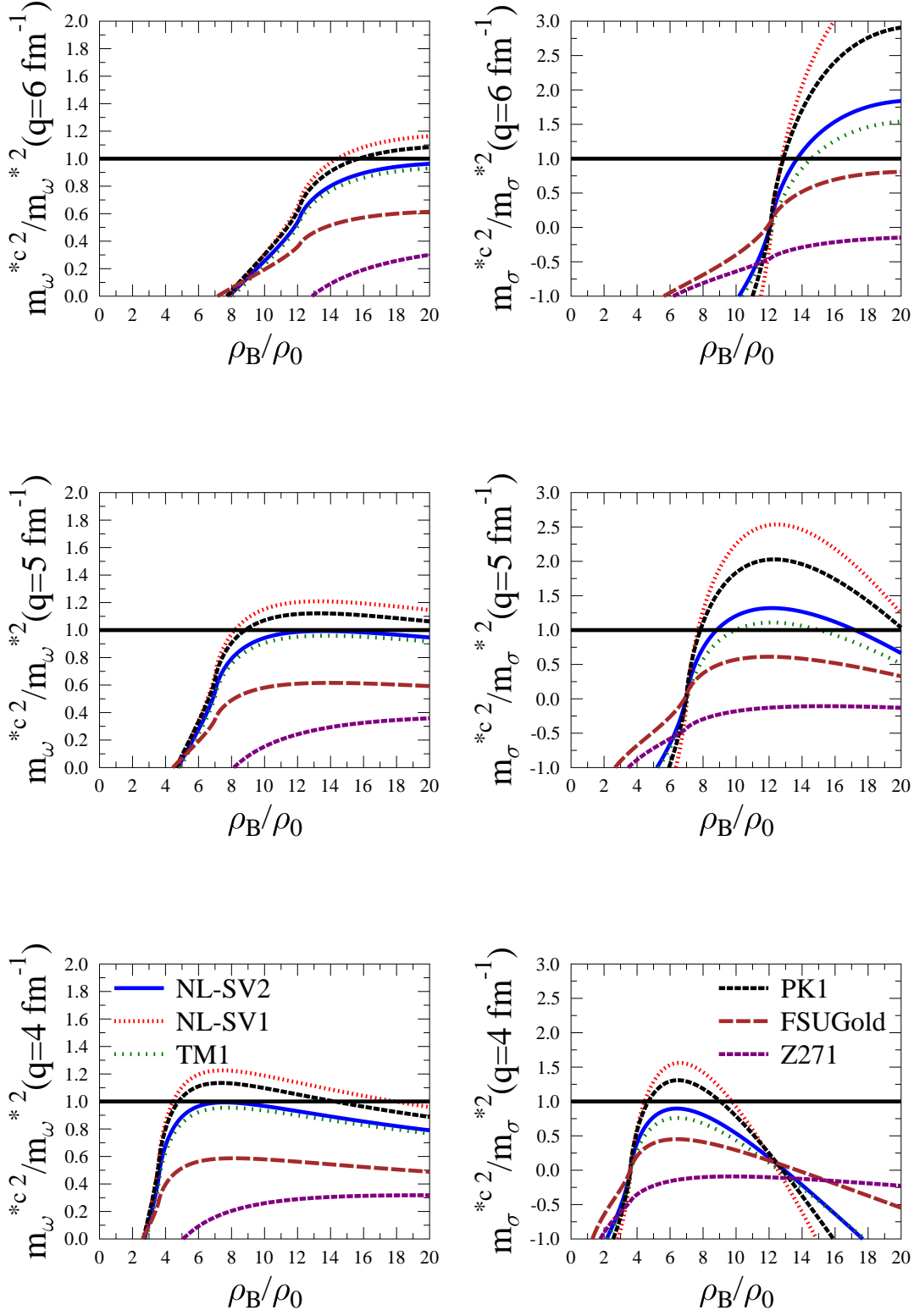


FIG. 8: $m_\sigma^{*2}/m_\sigma^{*2}$ and $m_\omega^{*2}/m_\omega^{*2}$ for some V-RMF parametrizations in Table III as functions of ρ_B/ρ_0 and with q varying as indicated.

density their effective omega meson mass becomes imaginary. This effect, as mentioned previously, appears as wild fluctuations in the critical effective sigma meson mass [8]. The presence of the c_3 parameter in the V-RMF model leads to the point that some parameter sets of this model are free of transverse instability while for some the critical density for longitudinal instability can be pushed to an unphysical region. Thus the presence of c_3 larger than a certain value can indeed remedy both instabilities.

B. Relativistic mean field model with mixing nonlinear terms

In this subsection, we discuss in more detail than in our previous work [8], the effect of the mixing nonlinear terms of some parameter sets of RMF model (E-RMF) that exist in the literature. The presence of these terms [8] provides additional terms in the energy density ε (Eq. (1)) with $-d_2\sigma V_0^2 - \frac{1}{2}d_3\sigma^2 V_0^2$, and in the longitudinal dielectric function ϵ_L (Eq. (2)) should be added with $4d_{SV}^L\Pi_{SV}$, where $\Pi_{SV} \equiv \Pi_M + 2d_{SV}^L\Pi_M^2 + 2d_{SV}^L\Pi_S\Pi_{00}$. The meson propagators therefore take the following forms

$$\begin{aligned} d_S &= \frac{g_\sigma^2}{q^2 + m_\sigma^{*2} + \Delta_{\sigma\omega}^2(q^2 + m_\omega^{*2})^{-1}}, \\ d_V^L &= \frac{g_\omega^2}{q^2 + m_\omega^{*2} + \Delta_{\sigma\omega}^2(q^2 + m_\sigma^{*2})^{-1}}, \end{aligned} \quad (13)$$

and now the scalar-vector coupling propagator is nonzero, i.e.,

$$d_{SV}^L = \frac{g_\omega g_\sigma \Delta_{\sigma\omega}}{(q^2 + m_\omega^{*2})(q^2 + m_\sigma^{*2}) + \Delta_{\sigma\omega}^2}, \quad (14)$$

where the effective meson masses become

$$\begin{aligned} m_\sigma^{*2} &= \frac{\partial^2 \epsilon}{\partial^2 \sigma} = m_\sigma^2 + 2b_2\sigma + 3b_3\sigma^2 - d_3V_0^2, \\ m_\omega^{*2} &= -\frac{\partial^2 \epsilon}{\partial^2 V_0} = m_\omega^2 + 3c_3V_0^2 + 2d_2\sigma + d_3\sigma^2, \\ \Delta_{\sigma\omega} &= -(\partial^2 \epsilon / \partial \sigma \partial V_0) = 2d_2V_0 + 2d_3\sigma V_0. \end{aligned} \quad (15)$$

These terms also modify m_σ^{*2c} in Eq. (11) into

$$m_\sigma^{*2c} = - \left[\frac{2g_\sigma^2(\Pi_S\Pi_T - \Pi_M^2 + \Pi_S\Pi_{00})(1 + \lambda_1)}{(\Pi_T + \Pi_{00})(1 + \lambda_2)} + q^2 \right], \quad (16)$$

while the corrections due to the mixing nonlinear terms are represented by

$$\begin{aligned}\lambda_1 &= \frac{1}{(\Pi_S \Pi_T - \Pi_M^2 + \Pi_S \Pi_{00})} (\delta_{\sigma\omega} [\Pi_M^2 - \Pi_S \Pi_{00}]), \\ \lambda_2 &= \frac{1}{(\Pi_T + \Pi_{00})} \left(\delta_{\sigma\omega} \Pi_T + \frac{4g_\omega g_\sigma \Pi_T \delta_{\sigma\omega}}{\Delta_{\sigma\omega}} \left[\Pi_M + \frac{2g_\omega g_\sigma \delta_{\sigma\omega}}{\Delta_{\sigma\omega}} (1 - \delta_{\sigma\omega}) [\Pi_M^2 - \Pi_S \Pi_{00}] \right] \right),\end{aligned}\tag{17}$$

with

$$\delta_{\sigma\omega} = \frac{\Delta_{\sigma\omega}^2}{(q^2 + m_\omega^{*2})(q^2 + m_\sigma^{*2})}.\tag{18}$$

It is clear that if $\lambda_1 = \lambda_2 = 0$, these terms do not affect the critical sigma meson mass. If both λ 's are not equal to zero, the critical sigma meson mass reduction or increase depends on the sign and values of both parameters. On the other hand, the actual effective masses of sigma and omega mesons still depend explicitly on the nonlinear mixing terms. As the representatives of the E-RMF model, the parameter sets G1 and G2 from Ref. [22], as well as FSUZ003 and FSUZ006 from Ref. [3] are used. The isoscalar parameters of these parameter sets can be seen in Table IV. The λ_1 , λ_2 , $m_\sigma^{*2} c / m_\sigma^2$ and $m_\omega^{*2} / m_\omega^2$ of the representative parameter sets for the case $q = 5\text{fm}^{-1}$ are shown in Fig. 9. In this case, the maximal values are $\lambda_1 \approx 2.5\%$ and $\lambda_2 \approx 15\%$ of the total contributions. Both are obtained using the G1 parameter set. This implies that the mixing nonlinear terms do not significantly affect the critical effective mass of the sigma meson. This can be seen from the lower left panel of Fig. 9. $m_\sigma^{*2} c / m_\sigma^2$ of the G1 parameter set is significantly lower than those of the other parameter sets, merely because it produces significantly smaller g_σ and g_ω compared to them (see Table IV). However, the significant effect of mixing nonlinear terms in the actual effective mass of the sigma meson can be seen in the right panel of Fig. 9. For the transverse mode, it is clear that G2 has an instability region because its c_3 is critical, i.e., produces the maximal effective mass of the omega meson, equal to the critical value. If the parameter c_3 is larger than this value like for the other E-RMF parameter sets, the instability disappears. For the longitudinal mode, the appearance of instability is merely determined by the effective sigma meson mass. The combination of b_2 , b_3 , and d_3 of each parameter set leads to $m_{\sigma\text{G1}}^{*2} < m_{\sigma\text{FSUZ003}}^{*2} < m_{\sigma\text{G2}}^{*2} < m_{\sigma\text{FSUZ006}}^{*2}$ (right lower panel of Fig. 9). Thus the critical density $\rho_c^{\text{G1}} < \rho_c^{\text{FSUZ003}} < \rho_c^{\text{G1}} < \rho_c^{\text{FSUZ006}}$. The large and positive value of b_3 is still

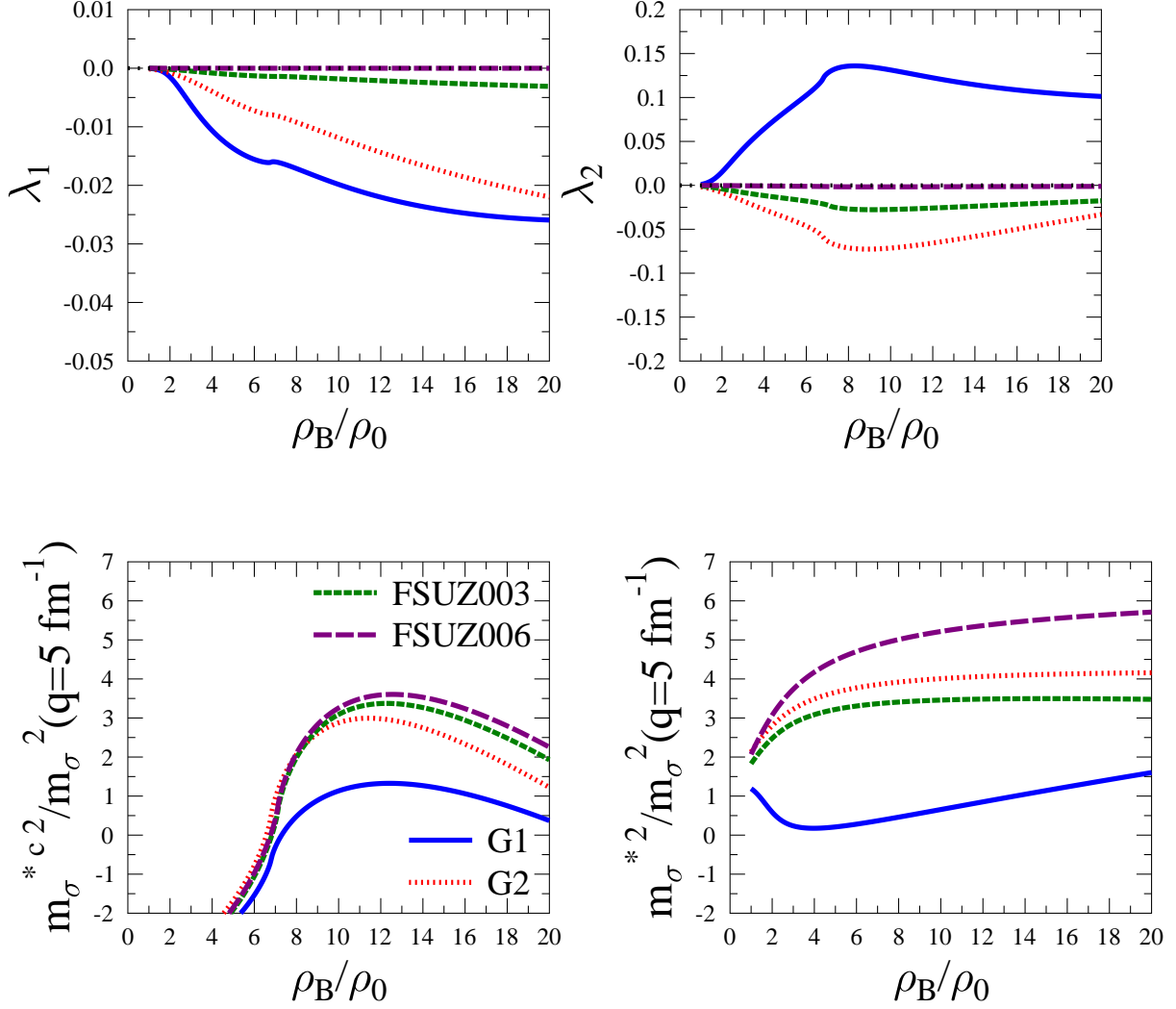


FIG. 9: λ_1 (in left upper panel), λ_2 (in the right upper panel), m_σ^{*2}/m_σ^2 (in the left lower panel) and m_ω^{*2}/m_ω^2 (in the right lower panel) for some E-RMF parameterizations and $q = 5\text{fm}^{-1}$.

the way to push the longitudinal instability to unphysical regions, but in the E-RMF model, the value of the critical b_3 need not be too large, because its contribution can be partly substituted not only by that of b_2 but also by that of d_3 . These facts can be understood by comparing Fig. 10 with nonlinear parameters in Table IV. Another interesting finding is that if we observe the parameters of G2 in Table IV, even its b_3 is negative and its absolute value is relatively large, but other contributions from b_2 and d_3 produce sufficient balancing contributions, avoiding this parameter set to have an imaginary effective sigma meson mass.

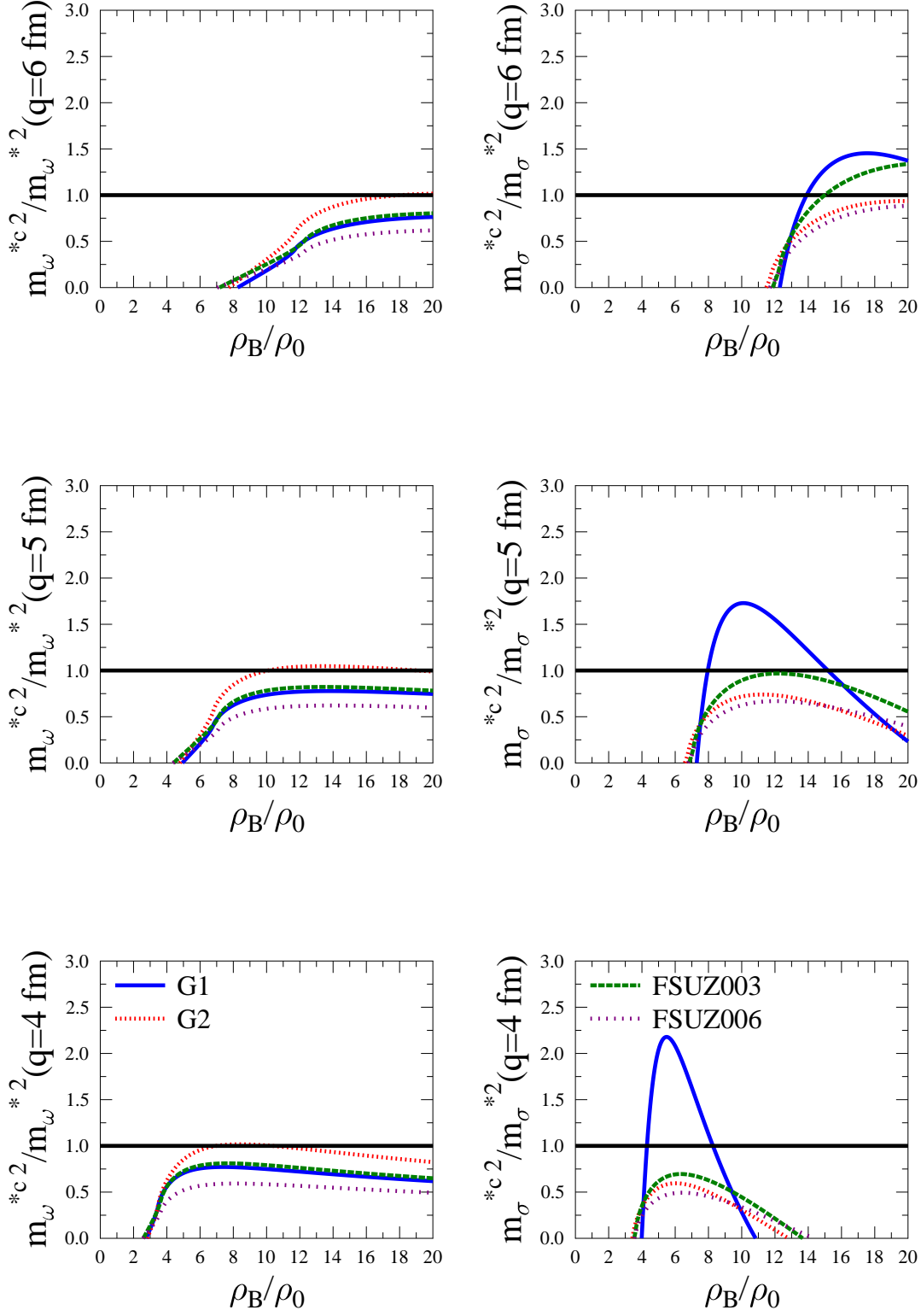


FIG. 10: $m_{\sigma}^{*2}/m_{\sigma}^{*2}$ and $m_{\omega}^{*2}/m_{\omega}^{*2}$ of some E-RMF parameterizations of Table IV as functions of ρ_B/ρ_0 and for some q values as indicated.

TABLE IV: Isoscalar parts of some E-RMF model parameter sets.

| Parameter | G1 | G2 | FSUZ003 | FSUZ006 |
|------------|--------|--------|---------|---------|
| g_σ | 9.87 | 10.49 | 10.76 | 11.02 |
| g_ω | 12.13 | 12.76 | 14.11 | 14.66 |
| b_2 | -15.09 | -24.89 | -9.72 | -4.65 |
| b_3 | -47.69 | 3.56 | 21.80 | 60.28 |
| c_3 | 86.41 | 71.71 | 198.25 | 462.64 |
| d_2 | -1.15 | -11.26 | -2.21 | -0.17 |
| d_3 | -32.56 | 4.19 | 11.69 | 1.38 |

IV. CONCLUSION

Based on the fact that the critical effective masses of the sigma and omega mesons (m_σ^{*2c} and m_ω^{*2c}) depend on the g_σ and g_ω coupling constants but are insensitive to the values of the b_2 , b_3 , and c_3 parameters, while the actual effective masses of the sigma and omega mesons (m_σ^{*2} and m_ω^{*2}) have opposite properties, we derive criteria to estimate the values of isoscalar nonlinear terms of the standard RMF model that produce a stable EOS at high densities. The minimal requirement on the standard RMF model free from transverse mode instability at high densities is that the quartic vector nonlinear parameter should exist and have a value of $c_3 > 71$. This value corresponds to the quartic scalar nonlinear parameter b_3 close to or larger than zero. The longitudinal mode instability cannot fully disappear but can be pushed to unphysical densities by taking b_3 relatively large and positive, for example, $b_3 \geq 20$, where in our chosen test parameter set, it corresponds to $c_3 \geq 160$. In this case, the critical density for the instability region can be pushed to $\rho_c \geq 23 \rho_0$. In usual applications, for examples neutron stars, supernova matter, etc., the density remains below $10\rho_0$, so that for these applications it seems sufficient to choose a parameter set with b_3 slightly lower than 20 is sufficient. We have also found that the parameter set of the standard RMF model with a stable nuclear matter EOS at high density is consistent with the experimental data of Ref. [12] and the microscopic calculation of Ref. [13].

The criteria has been used to systematically analyze the high density longitudinal and transverse modes instabilities of standard RMF models. We have shown that both parameter

sets unstable at high densities and stable ones exist. The reason behind this fact has been explained quantitatively and the crucial role of the isoscalar vector nonlinear term has also been clearly demonstrated. The effect of the mixing nonlinear terms of some parameter sets of the RMF model (E-RMF) has been also studied. Due to the contribution of these parameters to the actual effective masses of the sigma and omega mesons (m_σ^{*2} and m_ω^{*2}) are changed, while the critical effective masses of sigma meson (m_σ^{*2c}) are affected only weakly. The stability of both modes can be achieved more easily compared to V-RMF because the thresholds of the critical values of c_3 and b_3 parameters of this model can be lower than those of V-RMF.

ACKNOWLEDGMENT

A. S. would like to thank M. M. Sharma for useful exchange of ideas connected with this work. A.S. also acknowledges financial support from DAAD and Universitas Indonesia. He is grateful for the kind hospitality during his stay in Institut für Theoretische Physics at Universität Frankfurt.

-
- [1] G. A. Lalazissis, S. Karatzikos, R. Fossion, D. Pena Arteaga, and P. Ring, Phys. Lett. B **671**, 36 (2009).
 - [2] M. M. Sharma, Phys. Lett. B **666**, 140 (2008).
 - [3] R. Kumar, B. K. Agrawal and S. K. Dhiman, Phys. Rev. C **74**, 034323 (2006).
 - [4] B. G. Todd-Rutel and J. Piekarewicz, Phys. Rev. Lett **95**, 122501 (2005).
 - [5] T. Klaehn *et. al*, Phys. Rev. C **74**, 035802 (2006).
 - [6] I. Sagert, M. Wietoska, J. Schaffner-Bielich and C. Sturm, J. Phys. G **35**, 014053 (2008).
 - [7] J. Piekarewicz, Phys. Rev. C **76**, 064310 (2007).
 - [8] A. Sulaksono, T. Mart, T. J. Buervenich and J. A. Maruhn, Phys. Rev. C **76**, 0431301(R) (2007).
 - [9] K. Lim and C. J. Horowitz, Nucl. Phys. A **501**, 729 (1989).
 - [10] B. L. Friman and P. A. Henning, Phys. Lett. B **206**, 579 (1988).
 - [11] H.-G. Doebereiner and P.-G. Reinhard, Phys. Lett. B **227**, 305 (1989).

- [12] P. Danielewicz, R. Lacey and W.G. Lynch, *Science* **298**, 1592 (2002).
- [13] A. Akmal, V.R. Pandharipande and D.G. Ravenhall, *Phys. Rev. C* **58**, 1804 (1998).
- [14] M. Rufa, P.-G. Reinhard, J. A. Maruhn, W. Greiner and M. R. Strayer, *Phys. Rev. C* **38**, 390 (1988).
- [15] G. Lalazissis, J. König and P. Ring, *Phys. Rev. C* **55**, 540 (1997).
- [16] M. M. Sharma, M. A. Nagarajan and P. Ring, *Phys. Lett. B* **312**, 377 (1993).
- [17] P.-G. Reinhard, *Rep. Prog. Phys* **52**, 439 (1989).
- [18] M. M. Sharma, A. R. Farhan and S. Mythili, *Phys. Rev. C* **61**, 054306 (2000).
- [19] Y. Sugahara and H. Toki, *Nucl. Phys. A* **579**, 557 (1994).
- [20] W. Long, J. Meng, N. VanGiai and S.-G. Zhou, *Phys. Rev. C* **69**, 034319 (2004).
- [21] C. J. Horowitz and J. Piekarewicz, *Phys. Rev. Lett* **86**, 5647 (2001).
- [22] R. J. Furnstahl, B. D. Serot and H. B. Tang, *Nucl. Phys. A* **598**, 539 (1996); *Nucl. Phys. A* **615**, 441 (1997).